Sputtered YSZ based protective thin films for SOFCs

A. L. Shaula*[1], J. C. Oliveira[1], V. A. Kolotygin[2], V. V. Kharton[2] and A. A. Cavaleiro[1]

Protective $Zr(Y)O_{2-\delta}$ based films, deposited using magnetron sputtering, onto apatite type ceramics, were appraised for potential applications in solid oxide fuel cells with silicate based solid electrolytes, where performance may suffer from surface decomposition processes in reducing atmospheres. While as prepared $Zr(Y)O_{2-\delta}$ films without copper additive were already crystallised and single phase, fresh Cu containing $Zr(Y)O_{2-\delta}$ are essentially amorphous, requiring high temperature treatment in air for crystallisation. Deposition rate of 0·50–0·75 μm h^{-1} at sputtering power of 300 W was achieved. Surface morphology studies using atomic force microscope revealed typical film structures with small (<50 nm) grains. The hardness of films decreases from 15·8 to 8·4 GPa with increasing copper content. Polarisation studies of electrochemical cell with cermet anodes, applied over protective films, suggested that electrochemical reaction is essentially governed by oxygen anion transfer from zirconia phase and/or hydrogen oxidation in vicinity of zirconia film surface. Copper incorporation into $Zr(Y)O_{2-\delta}$ film leads to higher anode resistivity.

Keywords: Yttria stabilised zirconia, Magnetron sputtering, Thin film, Hardness, Apatite, Solid oxide fuel cell

Introduction

Solid oxides with predominant oxygen ionic conductivity are key materials for high temperature electrochemical applications, such as solid oxide fuel cells (SOFCs), gas electrolysers and electrocatalytic reactors for natural gas conversion, oxygen sensors and pumps.[1–4] These devices provide important advantages compared to conventional industrial processes. For instance, the use of SOFCs for electrical power generation leads to a high energy conversion efficiency, environmental safety and fuel flexibility including the prospects of direct operation with natural gas. Before commercialisation, solid oxide electrolytes should satisfy many aspects, such as high ionic conductivity, minimum electronic transport, moderate thermal expansion and thermodynamic stability in wide ranges of oxygen partial pressure and temperature. Also, the costs associated with raw materials and processing technologies should be as low as possible.

Relatively high oxygen ionic transport in combination with moderate thermal expansion and low electronic conduction in a wide range of the oxygen chemical potential was recently reported for lanthanum apatite type silicates.[5–12] At 773–873 K, the conductivity of some ceramics is higher than ionic conductivity of an yttria stabilised zirconia (YSZ) and similar to that of gadolinia doped ceria.[10–12] Si based electrolytes are promising materials considering the low cost of raw materials and well developed technologies for SiO_2 based film processing in the electronic industry.

However, the apatite type silicates are characterised by moderate stability in reducing atmospheres at elevated temperatures.[13,14] The long term stability measurements of apatite type $La_{10-x}Si_{6-y}Al_yO_{27-3x/2-y/2}$ oxides in reducing conditions showed a slow irreversible degradation of these silicates at temperatures above 1100 K, associated with reduction to SiO and its volatilisation from the surface layers.[13] Therefore, working temperatures as low as approximately 800–1000 K are needed to avoid silicon oxide volatilisation.[13]

An alternative way to stabilise the apatite type silicates under SOFC anode side operating conditions is to apply a thin oxide ion conducting film onto the apatite membrane, so this layer will act as a protective barrier between an electrolyte and reducing gas mixture. Yttria stabilised zirconia was selected for this purpose because of its high oxygen ionic conductivity, excellent electrolytic domain and stability in reducing environments.[4,15,16] The magnetron sputtering deposited YSZ thin films were already tested as electrolyte material for $La(Sr)MnO_{3-\delta}$–YSZ cathodes and Ni–YSZ anodes.[17–19] But there is no information on the magnetron sputtered YSZ thin films over the apatite type lanthanum silicates. Hence, the present work deals with the deposition of YSZ based films onto $La_{9·83}Si_{4·5}Al_{1·5}O_{26}$ (LSAO) membranes, which show relatively high oxygen ionic

[1]Department of Mechanical Engineering, SEG-CEMUC, University of Coimbra, 3030-788 Coimbra, Portugal
[2]Department of Ceramics and Glass Engineering, CICECO, University of Aveiro, 3810-193 Aveiro, Portugal

*Corresponding author, email ashaula@cv.ua.pt

Published by Maney on behalf of the Institute
Received 17 March 2009; accepted 4 May 2009
DOI 10.1179/174329409X455430

conductivity and excellent durability in air,[12–14] and measurements of electrochemical properties of such bilayer solid electrolyte in contact with cermet anode based on Ni, YSZ and $Ce_{0·8}Gd_{0·2}O_{2-\delta}$ (50 : 30 : 20 wt-%). Cu containing $Zr(Y)O_{2-\delta}$ films were also tested since copper (low cost material with easy processing technology) addition was shown to improve the anode adhesiveness and durability without significant resistivity increase.[20,21]

Experimental procedures

Dense single phase LSAO ceramics were prepared by a standard solid state synthesis route from stoichiometric amounts of high purity La_2O_3, SiO_2 and $Al(NO_3)_3.9H_2O$. Following prereaction at 1273–1473 K and ball milling, ceramic samples were sintered at 1873–1973 K during 10 h in air. The density of gas tight samples was higher than 95% of their theoretical density. Gas tightness of membranes was checked by the absence of air penetration when one of membrane sides is kept at atmospheric pressure and covered with a thin layer of ethylic alcohol, while air is supplied to the other side under pressure of 2–3 bar. The absence of air bubbles within the ethylic alcohol layer indicates the gas tightness of ceramic membranes.

All the films were deposited by radio frequency (rf) magnetron sputtering in an Edwards E306A coating system. The sputtering source was driven by a 13·56 MHz rf power supply. To produce $Zr(Y)O_{2-\delta}$ films, a 99·95% pure ZrO_2 (10–15 wt-%Y_2O_3, 10 cm diameter, 6 mm thickness) target from CERAC was used. Two or four copper plates (10 × 15 mm each, 2 mm thickness) were placed onto this target close to the magnetron ring, if composite $Zr(Y)O_{2-\delta}$–Cu films were needed (YSZ–Cu2 and YSZ-Cu4 respectively). The coatings were sputter deposited onto Si (10 × 5 mm, 2 mm thick), steel (diameter of 5 mm, 5 mm thick) and LSAO (diameter of 2 cm, 1 mm thick) substrates at a pressure of ~0·8 Pa applying an rf bias to the target with a power of 300–500 W for 1–3 h.

The elemental composition of the coatings was determined by electron probe microanalysis (EPMA) using a Cameca SX-50 apparatus with an acceleration voltage of 15 kV (40 mA) and ZrO_2, Y_2O_3 and Cu_2O standards. The low angle X-ray diffraction (XRD) patterns (Cu K_α, incidence angle 2°, 2Θ=10–70°, step 0·02°, 1 s/step) were taken using a Philips X'pert diffractometer.

The cross-section and surface of the coatings were examined in a Hitachi S-4100 (25 kV) scanning electron microscope (SEM) coupled with energy dispersive X-ray detector for energy dispersive spectroscopy (EDS). The morphology of surface was also assessed using molecular imaging PicoLE atomic force microscope (AFM). Measurements were carried out in ac mode using Si probes with tip radius <10 nm, highly doped in order to dissipate surface charge.

Micro-, ultramicro- and nanohardness tests were performed by means of a HMV microhardness tester (Vickers), a Fisherscope H100 (Vickers) and a NanoTest equipment (Berkovich), correspondingly. Each hardness value is a result of at least 16 indentations.

A mixture of Ni, 8YSZ and $Ce_{0·8}Gd_{0·2}O_{2-\delta}$ (50 : 30 : 20 wt-%) was selected as the anode (Ni–YSZ–CGO) for polarisation studies, taking into account

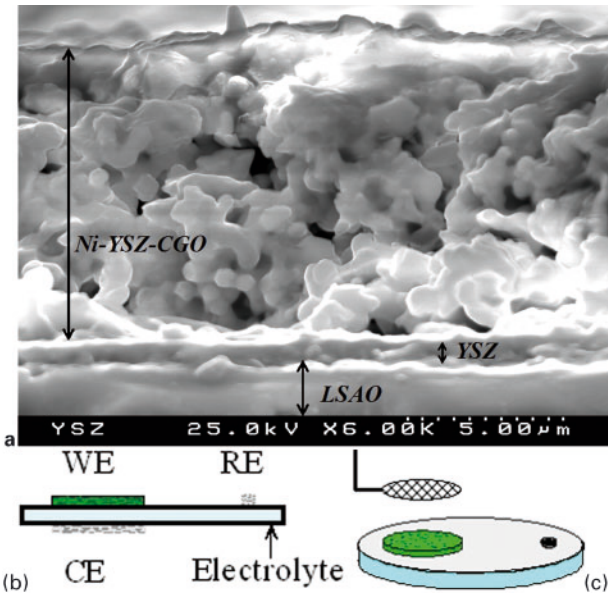

1 ***a*** **cross-section image of Ni–YSZ–CGO anode annealed onto surface (covered with sputterdeposited YSZ film) of LSAO membrane, and *b*, *c* scheme of three-electrode measuring cell**

relatively low overpotential/current ratio values reported previously for this composition.[22] The commercially available YSZ (Tosoh) and CGO (Rhodia) powders were used. Nickel was first added as NiO, by thermal decomposition of $Ni(NO_3)_2.6H_2O$ (Aldrich), and later reduced to metal. The powder mixture was ball milled and its alcohol based paste was screen printed (25 mg cm^{-2}) onto the surface (covered with sputter deposited YSZ film of ~1 μm in thickness) of LSAO membranes. The anode layer was annealed at 1523 K during 1 h in air (Fig. 1*a*). The Cu–YSZ (40 : 60 vol.-%) cermet anode was prepared from CuO and YSZ powders in the same way and annealed onto $La_{10}Si_5AlO_{26·5}$ membranes at 1273 K during 1 h in air.

The anodic overpotential η dependences on the current density i were studied by the three-electrode technique with porous Pt counter and reference electrodes (CE and RE, Fig. 1*b*), using an Autolab PGSTAT302 instrument. A platinum mesh current collector was used for the working electrode (WE), as illustrated by Fig. 1*c*. The polarisation measurements were performed at 973–1123 K in flowing wet $10H_2$–$90N_2$ gas mixtures; the oxygen partial pressure $p(O_2)$ was measured by an YSZ oxygen sensor. The air (12·5 mL min^{-1}) and wet $10H_2$–$90N_2$ (50 mL min^{-1}) flowrates were controlled by a Bronkhorst mass flow controller. The overpotential reproducibility error for the similar anodes prepared under identical conditions was 15–25%; the deviation from initial overpotential values after 120 h of testing was lower than 10%.

Results and discussion

After deposition, YSZ films appeared transparent and remain this way after annealing at 1273 K during 1 h in air, whereas as deposited Cu containing YSZ coatings were black. The heat treatment did not change their colour considerably. The nominal composition of YSZ target (10–15 wt-%Y_2O_3) suggests formula representation as somewhat between $Zr_{0·89}Y_{0·11}O_{2-\delta}$ and

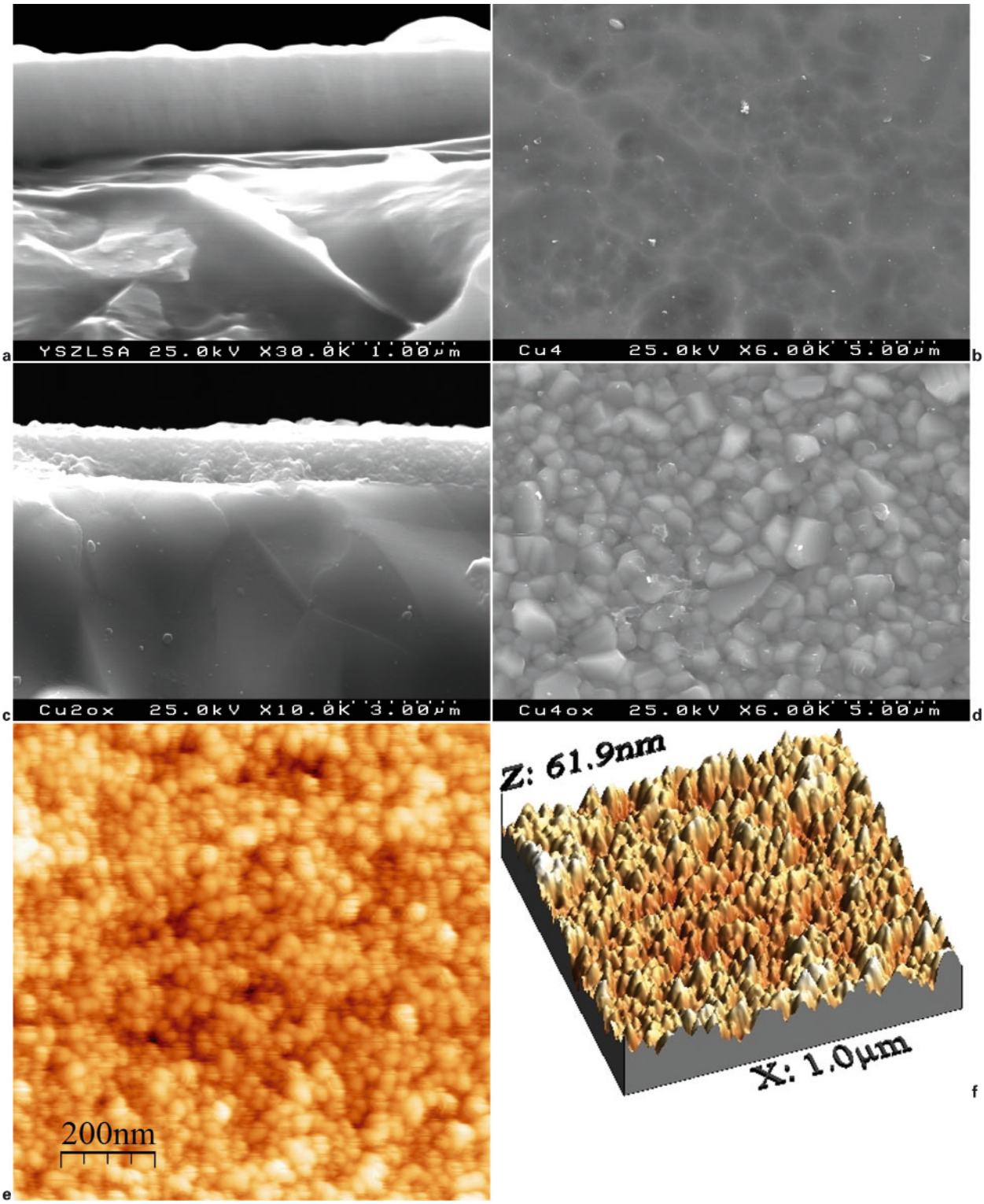

2 ***a*** **cross-section of as deposited YSZ film (2 h, 300 W),** ***b*** **surface of as deposited YSZ–Cu4 film,** ***c*** **cross-section of annealed YSZ–Cu2 film,** ***d*** **surface of annealed YSZ–Cu4 film,** ***e*** **surface of annealed YSZ film and** ***f*** **its three-dimensional representation: all coatings presented were deposited on LSAO substrates during 2 h using target power of 300 W**

$Zr_{0\cdot84}Y_{0\cdot16}O_{2-\delta}$. Table 1 presents the chemical composition of as deposited films, evaluated from EDS and EPMA data. Note that the chemical composition of YSZ coating is consistent with that of the target. The hardness values for YSZ, YSZ–Cu2 and YSZ–Cu4 films and LSAO ceramics are listed in Table 1. There is some difference between hardness values of LSAO ceramics for almost the same 'load' in the case of microhardness measurements and 'maximum load' in case of ultra-microhardness measurements (0·05 kg≈0·50 N). Such a discrepancy might be associated with the difference between these two methods: the latter one employs a so called depth sensing indentation technique and uses the curves of penetration *v.* load, whereas the former one is

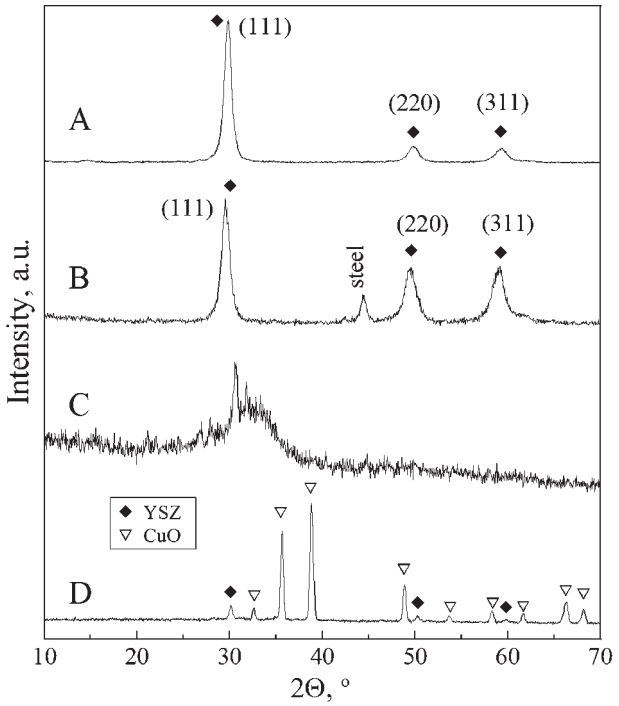

3 Low angle room temperature XRD patterns of YSZ films as deposited over *A* LSAO and *B* steel substrates, *C* YSZ–Cu2 film as deposited over LSAO substrate and *D* YSZ–Cu4 film deposited over LSAO substrate and annealed at 1000°C in air: all coatings presented were deposited during 2 h using target power of 300 W

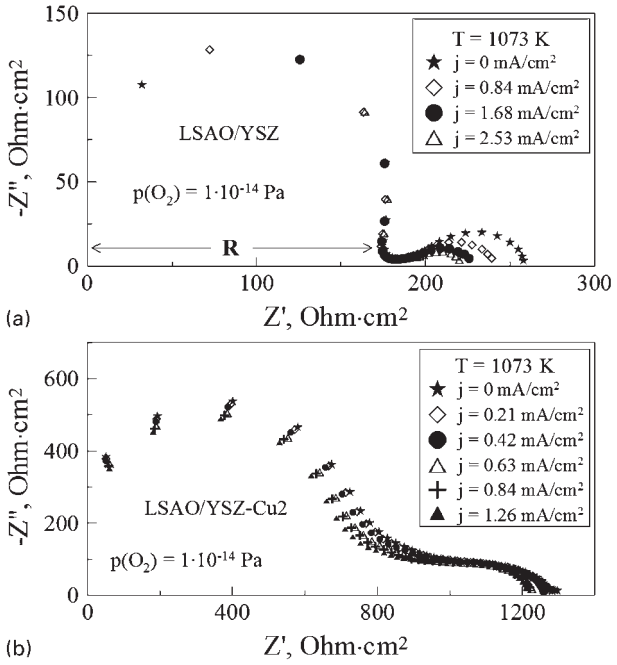

4 Impedance spectra for Ni–YSZ–CGO (50 : 30 : 20 wt-%) anode deposited onto protective *a* YSZ and *b* YSZ–Cu2 films, collected during polarisation measurements at 1073 K in flowing wet $10H_2$–$90N_2$ gas mixture: *R* corresponds to half-cell ohmic resistance

based on the length measurements of the X shaped cracks, caused by applying certain loads. The YSZ hardness (15·8±2·8 GPa) is in reasonable agreement with other magnetron sputtered YSZ coatings: 13·2,[23] 5·9–20·1,[24] 6·2 and 12·3,[25] and 12–19 GPa.[26] The hardness of the studied films decreases with incorporation of copper, which was also found by Musil *et al.*[23] for Zr–Cu–O magnetron sputtered films (8·0 GPa for 29 at.-%Cu).

In all cases (Cu free and Cu containing films), crack free, dense coatings on LSAO substrates were obtained, as demonstrate cross-section and surface SEM images (Fig. 2*a–d*). As deposited films have columnar morphology, similar to various YSZ films, deposited via both rf[27] and dc[28] magnetron sputtering. After annealing at 1273 K in air, the coatings are typically composed of relatively small grains (<1 μm for Cu containing films). The surface morphology AFM studies confirmed the dense structure of obtained YSZ based coatings (Fig. 2*e*). This top view shows that the annealed YSZ films consist of nanoscale grains (<50 nm). The corresponding three-dimensional image is given in Fig. 2*f*. The statistical analysis of this scan resulted in the following parameters: the average height R_z of the surface 33·0 nm, the root mean square roughness 8·0 nm and the average roughness 6·4 nm. These values are in a reasonable agreement with literature data.[24–26]

As expected, the thickness of coatings increases with rf power and deposition time. For the target power value of 300 W, which was selected as providing necessary growth rate and stable deposition, SEM images of Cu free and Cu containing YSZ films suggest deposition rate of about 0·50–0·75 μm h^{-1}. This is a relatively high velocity among those reported for both rf[29,30] and dc[28,31]

Table 1 Properties of LSAO ceramics and YSZ based films

Chemical composition of YSZ based films

YSZ	$Zr_{0·88±0·01}Y_{0·12±0·01}O_{2-\delta}$
YSZ–Cu2	$Zr_{0·89±0·01}Y_{0·11±0·01}O_{2-\delta}$–(0·67±0·03)$CuO_{1-\theta}$
YSZ–Cu4	$Zr_{0·88±0·01}Y_{0·12±0·01}O_{2-\delta}$–(2·32±0·15)$CuO_{1-\theta}$

Hardness values of LSAO ceramics

Microhardness		Ultramicrohardness		Nanohardness	
Load, kg	H_V, GPa	Maximum load, N	H_V, GPa	Maximum load, N	H_V, GPa
0·05	9·31±0·50	0·50	11·45±0·21	0·01	11·5±1·4
0·20	9·14±0·68	…	…	0·02	10·9±1·2
0·50	8·69±0·28	…	…	0·03	11·5±1·7
2·00	8·02±0·37	…	…	0·04	10·5±1·5

Nanohardness values of YSZ based films H_V, GPa

Maximum load, N	YSZ	YSZ–Cu2	YSZ–Cu4
0·01	15·8±2·8	9·8±0·9	8·4±0·7

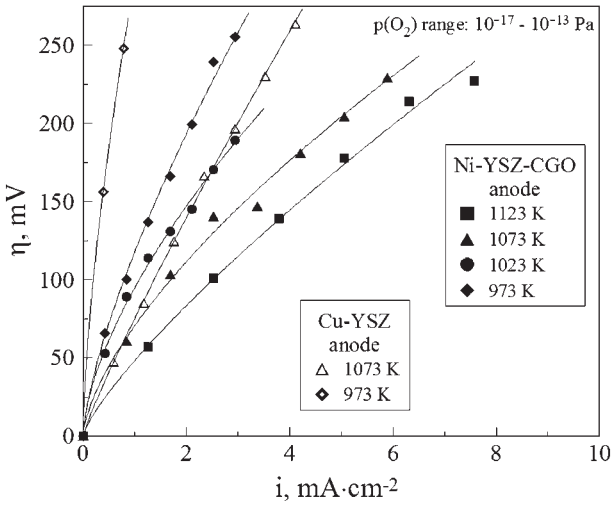

5 Overpotential–current dependences for Ni–YSZ–CGO (50 : 30 : 20 wt-%) anode deposited onto protective YSZ film, at 973–1123 K in flowing wet $10H_2$–$90N_2$ gas mixture: data are compared to Cu–YSZ cermet anode (40 : 60 vol.-%), annealed on $La_{10}Si_5AlO_{26·5}$ membrane, without protective interlayer

magnetron sputtered YSZ coatings. Note that the thickness of the films, estimated from SEM images, was systematically confirmed using Perthometer PRK profilometer with Perthometer S4P electronic module allowing an accuracy of $\sim$50 nm.

X-ray diffraction study of as deposited YSZ coatings indicated formation of the cubic fluorite type oxide, similarly to literature data on structural investigations of YSZ films prepared in similar deposition conditions.[31,32] Substitution of steel substrates with LSAO ceramics influences the intensity ratios of reflection peaks (Fig. 3*A* and *B*). Sputter deposition of YSZ–Cu films demonstrated formation of an amorphous phase for both Cu containing compositions, most likely, mixed with cubic fluorite type phase of YSZ (Fig. 3*C*). An amorphous structure was also recently reported for Zr–Cu–O films with 29 at.-%Cu.[21] The XRD patterns of YSZ–Cu coatings annealed at 1273 K for 1 h in air (Fig. 3*D*) are indicative of the presence of fluorite type $Zr(Y)O_{2-\delta}$ and copper oxides (mainly CuO).

The performance of Ni–YSZ–CGO anode annealed over YSZ film (which, in turn, was sputter deposited on LSAO membranes) was measured in reducing atmospheres of wet $10H_2$–$90N_2$ gas mixture. The impedance spectra (Fig. 4*a*) consisted of two semicircles (high and low frequency ones). The high frequency arcs are current independent and are attributed to the sum of ohmic resistances. The low frequency semicircles have a half-pear shape and typically shrink on increasing current through YSZ–LSAO between working (WE) and counter (CE) electrodes. These semicircles are associated with the electrode reaction involving in particular oxygen anion transfer at the interfaces between WE, YSZ coating and silicate electrolyte. The impedance values of the studied half-cells with Ni–YSZ–CGO anode, YSZ film and LSAO membrane at 973–1123 K are consistent with literature data on similar anode and film compositions,[18,19,33] although direct comparison is complicated due to temperature difference.

Note, however, that contrary to a reasonably good anodic performance of Ni–YSZ–CGO in contact with YSZ–LSAO system, substitution of Cu free YSZ protective thin film with Cu containing YSZ based coatings leads to about 8–10 times higher anode resistivity (Fig. 4*b*). Most likely, this can be associated to insufficient content of solid electrolyte phase (YSZ), even in the case of YSZ–Cu2 (Table 1). Hence, the oxygen ionic transport through these Cu containing films is almost totally blocked. Therefore, a significant decrease in copper concentration in Cu–YSZ composite is needed in order to deposit thin films with higher mixed oxide ion and electronic conductivity.

The overpotential at a fixed current density decreases, as expected, with increasing temperature (Fig. 5). The polarisation measurements at 973 K were repeated after a measurement cycle at 973–1123 K, during $\sim$120 h, and demonstrated slightly higher overpotential values in comparison with those of fresh anode. Nonetheless, the increase is modest (<10–15%). Energy dispersive spectroscopy studies showed no essential alteration, particularly no SiO_2 enrichment, in chemical composition of the YSZ coatings after such treatment in reducing conditions. The anode performance of the studied system is comparable to Cu–YSZ cermet anodes, deposited onto apatite type solid electrolyte membranes, without an intermediate YSZ layer (Fig. 5). Such behaviour indicates that the performance is essentially limited by oxygen anion transfer from the zirconia phase and/or hydrogen oxidation in the vicinity of zirconia surface; the interface between zirconia and silicate electrolyte seems to play no substantial role. The presence of YSZ interlayer and catalytically active nickel and ceria expands the electrochemical reaction zone.

Conclusions

Dense Cu free and Cu containing YSZ films were deposited by magnetron sputtering on LSAO substrates. As produced YSZ films without copper were already crystallised and single phase, while fresh Cu containing YSZ coatings are essentially amorphous. Their crystallisation was provided by a high temperature treatment in air. Deposition rate of 0·50–0·75 μm h^{-1} at sputtering power of 300 W was achieved. Surface morphology studies using AFM revealed typical film structures with small (<50 nm) grains. The hardness of films decreases from 15·8 to 8·4 GPa with increasing copper fraction. The overpotential–current characteristics of the studied system with Ni–YSZ–CGO anode are comparable to those with Cu–YSZ anode, also applied over apatite type solid electrolyte membranes, but without an intermediate YSZ film. These polarisation measurements suggest an applicability of this model, based on magnetron sputtering of protective YSZ films before the anode deposition, for the development of fuel cells with silicate electrolytes.

Acknowledgements

This work was supported by the FCT, Portugal (POCI program and grant SFRH/BPD/28913/2006) and by the MatSILC project (STRP 033410, CEC). Helpful discussions and experimental contributions, made by M. Evaristo and K. A. Yasakau, are gratefully acknowledged.

References

1. O. Yamamoto: *Electrochim. Acta*, 2000, **45**, 2423–2435.
2. S. P. S. Badwal and F. T. Ciacchi: *Adv. Mater*., 2001, **13**, 993–996.
3. J. B. Goodenough: *Ann. Rev. Mater. Res*., 2003, **33**, 91–128.
4. B. C. H. Steele: *J. Mater. Sci*., 2001, **36**, 1053–1068.
5. S. Nakayama, T. Kageyama, H. Aono and Y. Sadaoka: *J. Mater. Chem*., 1995, **5**, 1801–1805.
6. H. Arikawa, H. Nishiguchi, T. Ishihara and Y. Takita: *Solid State Ionics*, 2000, **136**–**137**, 31–37.
7. E. J. Abram, D. C. Sinclair and A. R. West: *J. Mater. Chem*., 2001, **11**, 1978–1979.
8. E. Rodriguez-Reina, A. F. Fuentes, M. Maczka, J. Hanuza, K. Boulahya and U. Amador: *J. Solid State Chem*., 2006, **179**, 522–531.
9. H. Yoshioka: *J. Alloys Compd*, 2006, **408**–**412**, 649–652.
10. V. V. Kharton, A. L. Shaula, M. V. Patrakeev, J. C. Waerenborgh, D. P. Rojas, N. P. Vyshatko, E. V. Tsipis, A. A. Yaremchenko and F. M. B. Marques: *J. Electrochem. Soc*., 2004, **151**, A1236–A1246.
11. L. Leon-Reina, E. R. Losilla, M. Martinez-Lara, S. Bruque and M. A. G. Aranda: *J. Mater. Chem*., 2004, **14**, 1142–1149.
12. A. L. Shaula, V. V. Kharton, J. C. Waerenborgh, D. P. Rojas and F. M. B. Marques: *J. Eur. Ceram. Soc*., 2005, **25**, 2583–2586.
13. A. L. Shaula, V. V. Kharton and F. M. B. Marques: *J. Solid State Chem*., 2005, **178**, 2050–2061.
14. A. A. Yaremchenko, A. L. Shaula, V. V. Kharton, J. C. Waerenborgh, D. P. Rojas, M. V. Patrakeev and F. M. B. Marques: *Solid State Ionics*, 2004, **171**, 51–59.
15. S. P. S. Badwal: *Solid State Ionics*, 2001, **143**, 39–46.
16. V. V. Kharton, F. M. B. Marques and A. Atkinson: *Solid State Ionics*, 2004, **174**, 135–149.
17. T. Tsai and S. A. Barnett: *Solid State Ionics*, 1997, **93**, 207–217.
18. P. Fedtke, M. Wienecke, M. C. Bunescu, T. Barfels, K. Deistung and M. Pietrzak: *J. Solid State Electrochem*., 2004, **8**, 626–632.
19. D. Kek, P. Panjan, E. Wanzenberg and J. Jamnik: *J. Eur. Ceram. Soc*., 2001, **21**, 1861–1865.
20. S. Park, J. M. Vohs and R. J. Gorte: *Nature*, 2000, **404**, 265–267.
21. Z Lu, L Pei, T. He, X. Huang, Z. Liu, Y. Ji, X. Zhao and W. Su: *J. Alloys Compd*, 2002, **334**, 299–303.
22. E. V. Tsipis, V. V. Kharton and J. R. Frade: *J. Eur. Ceram. Soc*., 2005, **25**, 2623–2626.
23. J. Musil, P. Zeman, M. Jirout, M. Sasek and R. Cerstvy: *Plasma Process. Polym*., 2007, **4**, S536–S540.
24. M. S. Wong, W. J. Chia, P. Yashar, J. M. Schneider, W. D. Sproul and S. A. Barnett: *Surf. Coat. Technol*., 1996, **86**–**87**, 381–387.
25. K. Goedicke, J. S. Liebig, O. Zywitzki and H. Sahm: *Thin Solid Films*, 2000, **377**–**378**, 37–42.
26. K. Koski, J. Holsa and P. Juliet: *Surf. Coat. Technol*., 1999, **120**–**121**, 303–312.
27. D. E. Ruddell, B. R. Stoner and J. Y. Thompson: *Thin Solid Films*, 2003, **445**, 14–19.
28. S. Jou and T. W. Chi: *Vacuum*, 2007, **81**, 911–919.
29. S. B. Amor, B. Rogier, G. Baud, M. Jacquet and M. Nardin: *Mater. Sci. Eng. B*, 1998, **B57**, 28–39.
30. B. Y. Liaw, R. E. Rocheleau and Q. H. Gao: *Solid State Ionics*, 1996, **92**, 85–89.
31. P. Briois, F. Lapostolle, V. Demange, E. Djurado and A. Billard: *Surf. Coat. Technol*., 2007, **201**, 6012–6018.
32. H. Tomaszewski, J. Haemers, J. Denul, N. D. Roo and R. D. Gryse: *Thin Solid Films*, 1996, **287**, 104–109.
33. P. K. Srivastava, T. Quach, Y. Y. Duan, R. Donelson, S. P. Jiang, F. T. Ciacchi and S. P. S. Badwal: *Solid State Ionics*, 1997, **99**, 311–319.